ACES Asian Chemical Editorial Society

DOI: 10.1002/cnma.201500210

CHEMNANOMAT
Full Paper

Aerogels

Carbon Aerogels Derived from Bacterial Cellulose/Polyimide Composites as Versatile Adsorbents and Supercapacitor Electrodes

Feili Lai,[a] Yue-E Miao,*[b] Lizeng Zuo,[a] Youfang Zhang,[a] and Tianxi Liu*[a, b]

Abstract: Hierarchically structured carbon aerogels consisting of one-dimensional carbon nanofibers and a three-dimensional carbon skeleton are prepared by sequential imidization and carbonization of bacterial cellulose/poly(amic acid) composite aerogels. The as-obtained carbon aerogels show excellent compressive properties, and can be directly used as versatile adsorbents for various liquids with superior sorption capacity and extraordinary recycling performance. Interestingly, the recycled carbon aerogels can still be used as electrode materials for supercapacitors with a high specific capacitance of 194.7 $F g^{-1}$ and excellent stability, which is attributed to the interconnected pores for fast ion diffusion, the maximized active site exposure for efficient charge adsorptions, and crosslinked carbon nanofibers for rapid electron transport. Therefore, this work provides a new strategy to develop multidimensional carbonaceous materials for both environmental and energy applications.

1. Introduction

For a long time, carbon-based materials have been regarded as reliable candidates to solve the severe environmental and water contamination issues.[1] In recent years, carbon aerogels, a promising class of carbon materials, have been applied in a broad range of essential applications, such as adsorption,[2] supercapacitors,[3] catalysis,[4] and hydrogen storage,[5] due to their low density, high porosity, adequate corrosion resistance, and high electrical conductivity.[6] Carbon aerogels consisting of one-dimensional carbon nanofibers with high aspect ratio are extremely intriguing for their unique aligned and intersected structures,[7,8] which satisfyingly provide maximized adsorptive and conductive properties. Recently, carbon nanofiber aerogels derived from carbonaceous nanofiber monolithic hydrogels were obtained through the combination of template-directed hydrothermal carbonization method, freeze drying technique and pyrolysis process, showing interconnected three-dimensional network structures with high sorption capacities toward various oils and organic solvents.[9] However, the fabrication processes not only bring potential environmental risks with the usage of sodium tellurite, but also are limited for mass production. Biomass, such as watermelon,[10] winter melon,[11] bagasse,[12] and plant cellulose,[13,14] on the other hand, has drawn great interest because of the rich reserves, renewability, and nontoxicity. Sun et al. synthesized porous carbon aerogels from renewable biomass waste of coconut shells via an easy and cost-effective simultaneous activation–graphitization route,[15] which provides short ion-diffusion channels for energy-storage devices attributed to their unique two-dimensional graphene-like structures. Nevertheless, the complicated composition of coconut shells, including cellulose, lignin, and pentosan, makes them hardly qualified as raw materials for further usages. Benefitting from the unique microbial fermentation process,[16] bacterial cellulose (BC) consisting of high-content superfine nanofibers with 40–60 nm in diameter is free of lignin/semicellulose, exhibiting large specific surface area, high crystallinity and porosity.[17,18] Nitrogen-doped carbon networks have been obtained through the carbonization of polyaniline-coated BC, which are directly used as excellent electrode materials for supercapacitors.[19] Wang et al. prepared ultra-light nanocomposite aerogels consisting of BC and graphene oxide, showing high sorption capacity (135–150 $g g^{-1}$) toward organic liquids.[20] However, the lack of strong crosslinking bonds/points between bacterial cellulose derived carbon nanofibers leads to poor shape-retention ability, which makes it critical to explore next-generation carbon-nanofiber-based aerogels with excellent mechanical properties to meet the ever-increasing demand.

[a] F. Lai, L. Zuo, Y. Zhang, Dr. T. Liu
State Key Laboratory of Molecular Engineering of Polymers
Department of Macromolecular Science
Fudan University
Shanghai 200433 (P.R. China)
E-mail: txliu@fudan.edu.cn

[b] Dr. Y.-E. Miao, Dr. T. Liu
State Key Laboratory of Modification of Chemical Fibers and Polymer Materials
College of Materials Science and Engineering
Donghua University
Shanghai 201620 (P.R. China)
E-mail: 12110440023@fudan.edu.cn

Supporting information for this article is available on the WWW under http://dx.doi.org/10.1002/cnma.201500210.

As one kind of the most widely used engineering plastics, polyimide (PI) materials possess a great deal of outstanding merits, such as excellent mechanical properties, high specific surface area, good thermal stability, and superior electrical conductivity.[21,22] The successful synthesis of polyimide/carbon nanofiber nanocomposites with superior mechanical properties indicates the great possibility of polyimide aerogels as self-supported sorbents.[23] Additionally, flexible nitrogen-doped carbon membranes fabricated by direct carbonization of heterocyclic polyimide membranes exhibit excellent volumetric capacitance of 159.3 F cm^{-3} at 1 A g^{-1}, high rate capability of 127.5 F cm^{-3} at 7 A g^{-1}, and long cycle life, further manifesting the potential applications of PI-based carbon materials as high-performance electrochemical electrode materials.[24]

In this work, carbon aerogels consisting of one-dimensional carbon nanofibers derived from BC and the three-dimensional carbon skeleton derived from PI were successfully synthesized through the sequential imidization and carbonization of BC/poly(amic acid) aerogels. Due to the excellent mechanical properties, porous structures and capillary effect of carbon nanofibers, the as-obtained carbon aerogels are directly used as versatile adsorbents, showing superior adsorption capacity and extraordinary recycling performance. Furthermore, high specific capacitance of 194.7 F g^{-1} at a current density of 0.5 A g^{-1}, good rate capability, and high capacitance retention of 94% after 5000 cycles are achieved when the carbon aerogels are employed as supercapacitor electrodes. Therefore, such versatile carbon aerogels may find potential applications in areas of not only adsorption but also high-performance energy-storage devices.

2. Results and Discussion

The typical preparation process is displayed in Scheme 1, and the details can be found in Experimental Section. Freeze-dried from BC/PAA suspensions in regular molds, white cylindric BC/PAA-50 aerogel is obtained as shown in Figure 1, displaying outstanding mechanical properties with a high compressive modulus of $\sigma = 0.63$ MPa at a set compressive strain of $\varepsilon =$ 60% (as the black line shows in Figure 1). Then, BC/PAA aerogel is turned into deep-yellow BC/PI aerogel, with the imidization reaction of –COOH and –NH_2 groups on PAA chains to form the six-membrane ring imide (i.e., –CO–NH–CO–).[26,27] Moreover, two obvious weight loss processes are observed for the BC/PI-50 aerogel from the TGA curve in Figure S1 in the Supporting Information. The weight loss of about 43% before 460 °C belongs to the decomposition of bacterial cellulose in air while the residual weight loss of about 57% at a higher temperature of about 530 °C is due to the decomposition of more thermally stable polyimide. Furthermore, due to the strong covalent bonds of the six-membrane ring imide, BC/PI-50 aerogel shows superior compressive modulus of $\sigma =$ 0.97 MPa at the set compressive strain of $\varepsilon = 60\%$ (as shown by the olive line in Figure 1), which is significantly higher than those of other fibrous aerogels.[28,29] In addition, the compressive modulus of BC/PI aerogels improves with the increase of PI content, which can be attributed to the rigid chains of polyimide and enhanced crosslinking effects between polyimide and ultrafine BC nanofiber networks. Therefore, the BC/PI-50 aerogel displays the most excellent mechanical property, revealing two characteristic deformation regimes:[30] a Hookean or linear elastic regime at $\varepsilon < 6\%$ and a densification regime at $\varepsilon > 6\%$. Though a lower compressive modulus of $\sigma = 67$ kPa at the set compressive strain of $\varepsilon = 60\%$ (as shown by the navy blue line in Figure 1) is achieved after carbonization of BC/PI-50 aerogel, BP-50 carbon aerogel can still endure 200 g weight without any deformation compared with the poor mechanical property of BP-0 carbon aerogel (as shown in Figure 2a), which is attributed to the reserved interconnected three-dimensional (3D) microstructure where the delicate carbon nanofibers are strongly supported by the PI-derived carbon skeleton. Interestingly, the robust BP-50 carbon aerogel can even stand on a dog's tail grass without any bending (Figure 2b), indicating its low density.

The microstructure of the carbon aerogels was observed by FESEM as shown in Figure 2c–2f. For BP-0 carbon aerogel, bacterial cellulose-derived carbon nanofibers with diameter of 40–

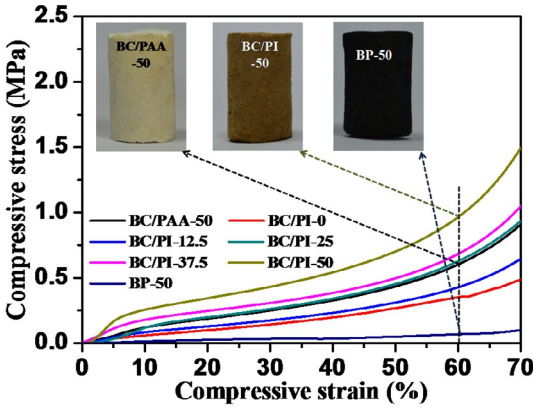

Figure 1. Compressive modulus (σ) versus compressive strain (ε) curves for BC/PAA-50, BC/PI-0, BC/PI-12.5, BC/PI-25, BC/PI-37.5, BC/PI-50 aerogels, and BP-50 carbon aerogel. Insets are the corresponding digital photographs of BC/PAA-50, BC/PI-50 aerogels, and BP-50 carbon aerogel.

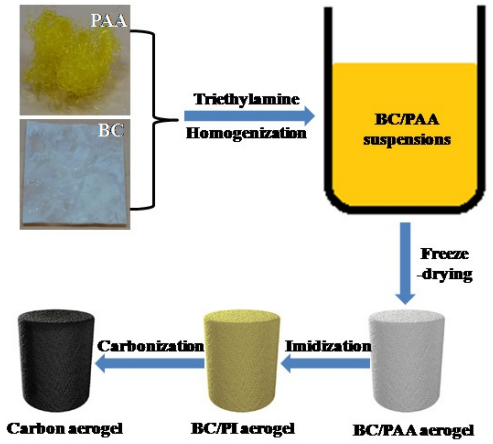

Scheme 1. Schematic for the preparation of BC/PAA aerogel, BC/PI aerogel, and BP carbon aerogel.

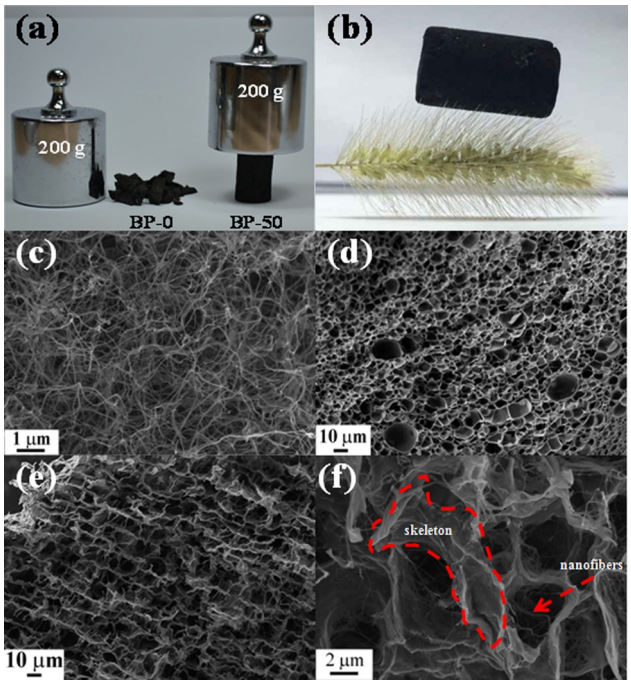

Figure 2. (a) Digital photographs of BP-50 and BP-0 carbon aerogels after loading of 200 g weight. (b) Digital photographs of BP-50 carbon aerogel standing on a dog's tail grass. Typical FESEM images of BP-0 (c), BP-100 (d), and BP-50 (e, f) carbon aerogels at different magnifications.

60 nm are intertwined into 3D networks. Nevertheless, the lacking of effective crosslinking leads to its poor mechanical properties. Oppositely, polyimide-based BP-100 carbon aerogel is consisted of unevenly enclosed shallow holes ranging from 5 to 20 μm, which would inevitably hinder the adsorption capacity toward oils/organic solvents. Completely differing from the morphologies of BP-0 and BP-100 carbon aerogels, BP-50 carbon aerogel exhibits cellular architectures with smaller and more uniform holes (≈10 μm). Moreover, the holes are highly interconnected with each other by the carbon skeleton originated from polyimide. As magnified in Figure 2 f, numerous bacterial-cellulose-derived carbon nanofibers cross between the carbon skeleton to further partition the holes into narrower spaces. In addition, the TEM image in Figure S2 also reveals that carbon nanofibers are closely connected between or even wrapped into the three-dimensional carbon skeleton. The unique structure consisting of 1D carbon nanofibers intertwined within the 3D carbon skeleton can be attributed to the successfully generated hydrogen bonds between bacterial cellulose nanofibers and PAA chains during the homogenizing process, which can not only increase the specific surface area, but also provide more ion diffusion and electron transport channels. BET analysis shows high specific surface area of 404.4 $m^2 g^{-1}$ for BP-50 carbon aerogel (Figure 3) with a relatively narrow pore size distribution in the range of 2 to 7 nm (inset of Figure 3), which is beneficial to achieve higher adsorption capacity and provide more active sites for charge adsorption.

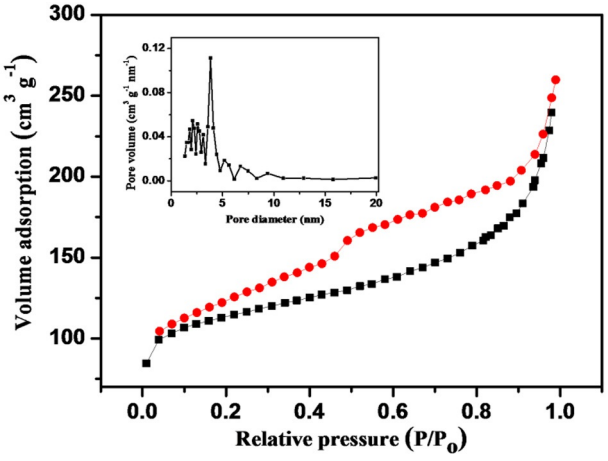

Figure 3. N_2 adsorption/desorption isotherms and the corresponding pore size distribution (inset) of BP-50 carbon aerogel.

XRD and XPS analyses were carried out as shown in Figure 4 to demonstrate the surface information of BP-50 carbon aerogel. The obvious peak at $2\theta = 25^\circ$ belongs to a typical (002) interlayer peak of graphite-type carbon (Figure 4 a). The atomic percentages of C and O in BP-50 carbon aerogel (Figure 4 b) are 81.9% and 14.1%, respectively, providing direct evidence of the high intensity of sp^2 C–C bond at about 284.6 eV (inset

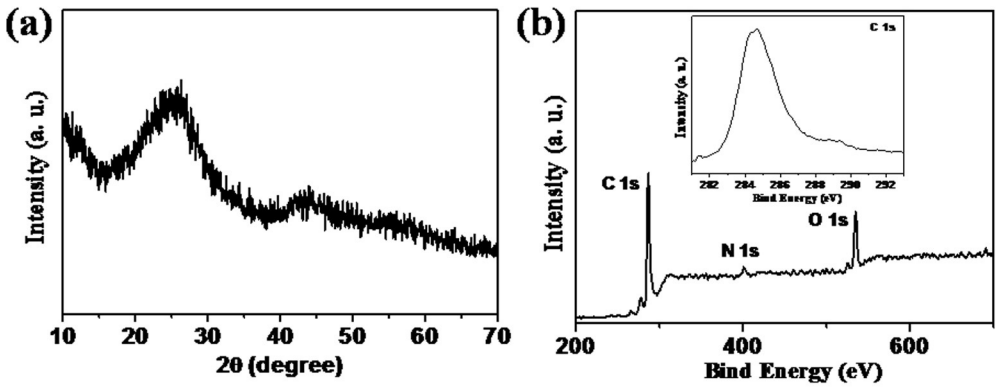

Figure 4. Surface information of BP-50 carbon aerogel: (a) XRD pattern; (b) XPS spectrum and the corresponding high-resolution C 1s spectrum.

of Figure 4b) due to the high-temperature carbonization of BC/PI aerogel. To emphasize, a high content (4%) of nitrogen atoms is observed, which may be derived from the precursor of polyimide. According to the previous report,[22] the precursor of polyimide (i.e., polyamide acid) contains enriched nitrogen atoms in the polymer chain, which can be hybridized into the carbon skeleton during the carbonization process and thus results in high efficiency of nitrogen doping.

The 3D porous structure of BP-50 carbon aerogel with low density, high hydrophobicity and excellent mechanical properties makes it an ideal candidate for removal of organic pollutants/oils. As shown in Figure 5a, heptane (stained with Sudan red 5B) floating on water was rapidly and completely adsorbed by cylindrical BP-50 carbon aerogel in several seconds even with slight contact between BP-50 carbon aerogel and the target pollutant (the dynamic process is shown in Movie S1, Supporting Information). Attributing to its low density and high hydrophobicity, the BP-50 carbon aerogel saturated with organic liquids can float on the surface of water, which makes it convenient to be recycled after adsorption of organic pollutants/oils.[31] In addition, when the BP-50 carbon aerogel is immersed in water to contact with chloroform (stained with Sudan red 5B) as shown in Figure 5b, chloroform is adsorbed from water completely and rapidly (with the dynamic process shown in Movie S2, Supporting Information).

In order to further study the adsorption efficiency of BP-50 carbon aerogel, a series of organic liquids, including petroleum products (e.g., pump oil), fats (e.g., colza oil), water-miscible solvents (e.g., isopropyl alcohol, benzyalcohol, DMF, acetone, and ethanol), and water-immiscible solvents (e.g., chloroform, toluene, octadecylene, heptanes, cyclohexane, and hexane), are studied as typical adsorbates. As shown in Figure 5c, the BP-50 carbon aerogel generally shows high adsorption efficiency toward almost all of the liquids with the uptake values at 10–40 times of its own weight, depending on the surface tension and viscosity of the adsorbed liquids. Furthermore, the crossed carbon nanofibers between the carbon skeleton can provide small pathways for liquid flow as well as enhance the capillary effect of carbon aerogels, thus contributing to the high adsorption capacity.[2,13] More importantly, the BP-50 carbon aerogel displays much higher adsorption capacity than those of the previously reported adsorbents (shown in Table 1), such as carbon nanofiber/carbon foam (25 times),[32] melon carbon aerogel (16–50 times),[11] conjugated microporous polymers (5–25 times).[33] In addition, the simple preparation process and earth-abundant precursors for BP-50 carbon aerogel jointly make it a cost-effective adsorbent for removal of organic pollutants/oils in water.

Recyclability of the adsorbents is another key criterion for environmental remediation applications. In order to demonstrate the recycling performance of BP-50 carbon aerogel, adsorption–combustion experiments are carried out by using ethanol as the adsorbate. As shown in Figure 6a, the BP-50 carbon aerogel still maintains a cylindrical shape with inherent multi-dimensional porous structures (Figure 6b) after the removal of ethanol by combustion in air. The adsorption capacity only drops by 5.1% after 5 cycles, indicating stable adsorption and recycling performance of BP-50 carbon aerogel.

Interestingly, the recycled BP-50 carbon aerogel (denoted as rBP-50 carbon aerogel) can still be applied as electrode materials for supercapacitors due to its good retention of porous microstructures after 5 adsorption–combustion cycles. The electrochemical performance of rBP-50 carbon-aerogel-based electrode is measured in 6 M KOH solution using a three-electrode configuration. In Figure 8a, the near-rectangular shape of CV

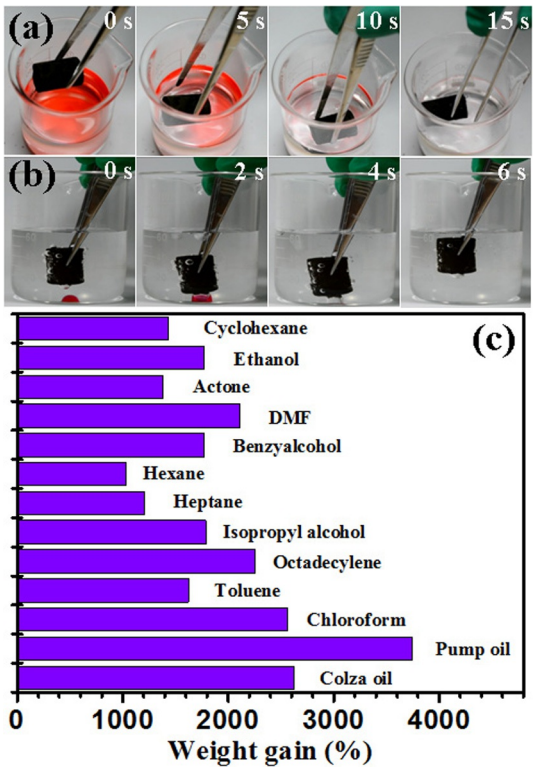

Figure 5. Adsorption of organic liquids by BP-50 carbon aerogel. (a) Photographs showing the adsorption process of BP-50 carbon aerogel toward heptane taken at time intervals of 5 s. The red heptane floating on water was stained with Sudan red 5B. (b) Photographs showing the adsorption process of chloroform by BP-50 carbon aerogel taken at time intervals of 2 s. The red chloroform droplet at the bottom of water was stained with Sudan red 5B. (c) Adsorption efficiency of BP-50 carbon aerogel toward various organic liquids. Weight gain here is defined as the weight ratio of the adsorbate to the dried BP-50 carbon aerogel.

Table 1. Comparisons of the adsorption capacity of various adsorbent materials.

Adsorbent materials	Adsorbed substances	Adsorption capacity [g g^{-1}]	Ref.
Corn stalk	gas oil	8	[35]
Expanded perlite	oil	3.2–7.5	[36]
Carbon nanofiber/carbon foam	motor	25	[32]
Carbon nanotube sponges	oil/organic solvents	80–180	[37]
Carbon nanotube aerogel	vegetable oil	40–80	[38]
Microporous polymers	oil/organic solvents	5–25	[33]
Sawdust	oil	3.77–6.4	[39]
Melon carbon aerogel	oil/organic solvents	16–50	[11]
BP-50 carbon aerogel	oil/organic solvents	10–40	This work

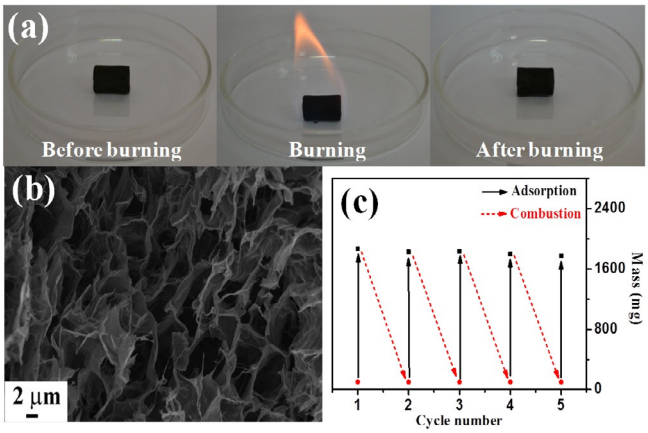

Figure 6. (a) Photographs showing the recycling process of BP-50 carbon aerogel via combustion. (b) Typical FESEM image of rBP-50 carbon aerogel after 5 adsorption–combustion cycles. (c) Recycling performance of BP-50 carbon aerogel for adsorption of ethanol by adsorption–combustion processes.

curves between −1 to 0 V is well-maintained with the increased scan rate, even at a high rate of 200 mV s^{-1}, indicating its ideal capacitive behavior. Furthermore, galvanostatic charge–discharge curves between −1 and 0 V exhibit a triangular shape without obvious internal resistance, which further proves the electric double layer capacitor characteristics of rBP-50 carbon aerogel. According to Equation (1) (see the Experimental Section), the specific capacitance of rBP-50 carbon aerogel is calculated to be 194.7 F g^{-1} at a current density of 0.5 A g^{-1}, which is much more outstanding than the previous works reporting on carbon-based electrode materials (Table 2), such as bacterial cellulose/lignin-based carbon aerogel,[34] and graphene/carbon aerogel.[21] The excellent electrochemical performance can be attributed to the following reasons: 1) First, the 3D structure of carbon aerogels with interconnected pores is beneficial to generate more channels for electrolyte diffusion into the inner spaces through the capillary effect. 2) Second, the high specific surface area of BP-50 carbon aerogel can obviously provide more active sites for efficient charge adsorption for fast charge and discharge processes. 3) The interconnected carbon nanofibers within the 3D carbon skeleton seem to act as "bridges" to more efficiently transport electrons in the interior structure of the electrode.

Benefiting from the above-mentioned merits of this multi-dimensional carbon aerogel, a high capacitance of 108.7 F g^{-1} is retained even at a high current density of 10 A g^{-1}, indicating the good rate capability of rBP-50 carbon aerogel (Figure 7c). Figure 7d shows a high capacitance retention of about 94% for rBP-50 carbon aerogel at a scan rate of 100 mV s^{-1} after 5000 cycles with similar shapes of the CV curves before and after cycling tests, as shown in the inset of Figure 7d, revealing excellent cycling stability of rBP-50 carbon aerogel for potential applications in long-term carbon-based electrode materials.

EIS analysis in the frequency ranging from 10 mHz to 100 kHz with 5 mV amplitude is taken to further investigate the fundamental resistance behavior of rBP-50 carbon aerogel as supercapacitor electrodes. As shown in Figure 8, a small equivalent series resistance of ca. 0.4 Ω without evident semi-

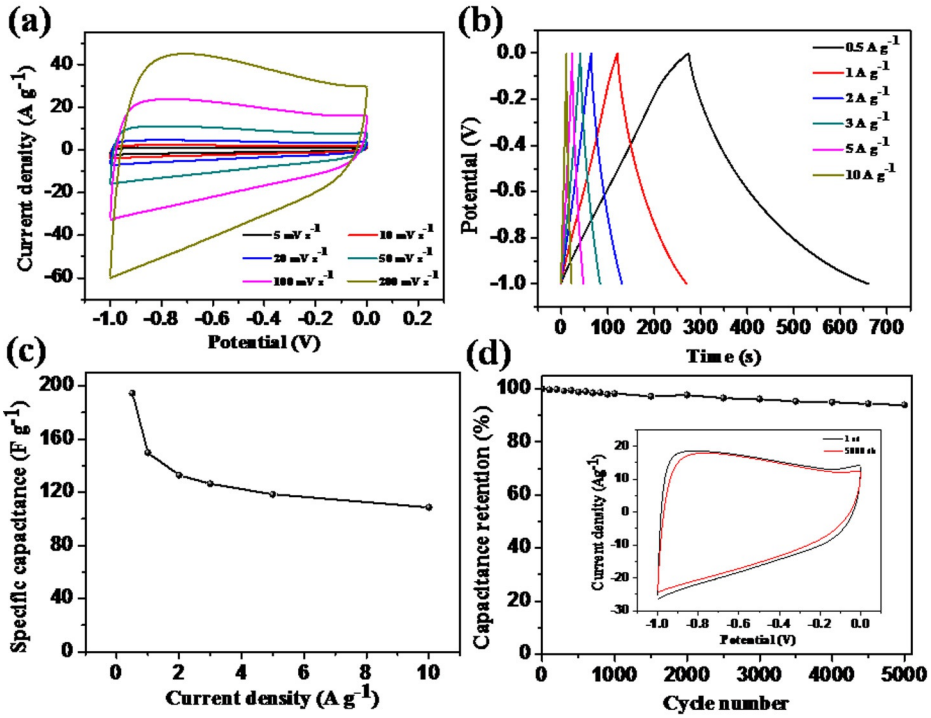

Figure 7. Electrochemical characteristics of rBP-50 carbon aerogel electrode in 6.0 M KOH aqueous solution by using a three-electrode system. (a) CV curves at different scan rates between 5 and 200 mV s^{-1}. (b) GCD curves at various current densities ranging from 0.5 to 10 A g^{-1}. (c) Specific capacitance of rBP-50 carbon aerogel at different discharge current densities. (d) Cycling performance of rBP-50 carbon aerogel at a constant scan rate of 100 mV s^{-1} with the inset showing the CV curves at the 1st and 5000th cycles.

Table 2. Comparisons of the specific capacitances of carbon-based electrode materials in a three-electrode system.

Carbon-based electrodes	Specific capacitance [F g^{-1}]	Conditions	Ref.
BC/lignin based carbon aerogel	124 (0.5 A g^{-1})	6 M KOH	[34]
Graphene/carbon aerogel	178.1 (1 A g^{-1})	6 M KOH	[21]
MOF[a]-derived carbons	251 (5 mV s^{-1})	1 M H_2SO_4	[40]
ZIF[b]-derived porous carbon	258.8 (0.1 A g^{-1})	6 M KOH	[41]
Activated carbon nanofiber	296 (2 mV s^{-1})	6 M KOH	[19]
CNT[c]-hollow carbon spheres	201.5 (0.5 A g^{-1})	6 M KOH	[42]
3D porous graphene	242 (2 A g^{-1})	1 M H_2SO_4	[43]
Bagasse derived carbon	136.6 (2 mV s^{-1})	6 M KOH	[12]
rBP-50 carbon aerogel	194.7 (0.5 A g^{-1})	6 M KOH	This work

[a] MOF: metal organic framework; [b] ZIF: zeolitic imidazolate frameworks; [c] CNT: carbon nanotubes.

circle is observed in the high frequency region for rBP-50 carbon aerogel, which corresponds to the charge transfer resistance. The vertical slope of the linear part in the low frequency region further indicates the low resistance of ion diffusion and electron transfer for rBP-50 carbon aerogel. Especially, the conductivity of rBP-50 is dramatically enhanced compared with rBP-100 carbon aerogel (Figure S3), further indicating the effectively reduced impedance of rBP-50 by the interpenetrated carbon nanofibers within the 3D carbon skeleton. Furthermore, slight increase of the resistance can be observed for rBP-50 carbon aerogel after 5000 cycles, indicating the excellent capacitive behavior of the electrode, which can be attributed to the porous structure constructed from 1D carbon nanofibers and the 3D carbon skeleton.

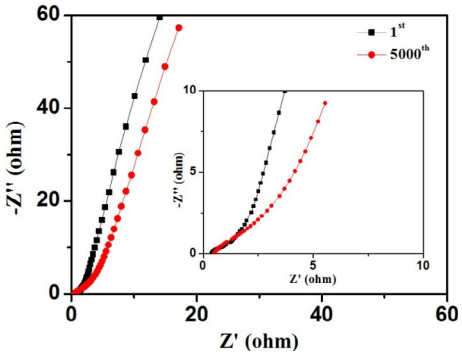

Figure 8. Nyquist plots for rBP-50 carbon aerogel in a frequency range from 10 mHz to 100 kHz during the life cycle tests. The inset shows the enlarged impedance spectra at the high-frequency region.

3. Conclusion

A facile method has been developed to produce multi-dimensional carbon aerogels by the successive imidization and carbonization of bacterial cellulose/poly(amic acid) aerogels. The obtained carbon aerogels composed of one-dimensional carbon nanofibers derived from bacterial cellulose and the three-dimensional carbon skeleton derived from polyimide display excellent mechanical strength with a compressive modulus of $\sigma = 67$ kPa at a set compressive strain of $\varepsilon = 60\%$, superior adsorption capacity, and excellent recycling performance. Furthermore, the recycled carbon aerogel can be directly used as the electrode material for supercapacitors with excellent electrochemical performance. As a result, we provide a new strategy to design multi-dimensional carbon aerogels with versatile functions, which may have potential applications in the fields of environmental remediation and energy storage.

4. Experimental Section

Materials

The bacterial cellulose pellicles (30×40 cm^2) were purchased from Hainan Yide Food Co. Ltd. 4,4′-oxidianiline (ODA), pyromellitic dianhydride (PMDA), triethylamine (TEA, 98%), *N,N*-dimethylacetamide (DMAc), cyclohexane, ethanol, acetone, *N,N*-dimethylformamide (DMF), benzylalcohol, hexane, heptanes, isopropyl alcohol, octadecylene, toluene and chloroform were all purchased from Sinopharm Chemical Reagent Co. Commercially available oil products (i.e., pump oil and colza oil) were used as probing liquids for oil sorption-capacity studies. All chemicals were of analytic grade and used without further purification.

Preparation of water-soluble poly(amic acid) (PAA)

The polycondensation process of water-soluble PAA (the precursor of PI) follows our previous work.[21] Briefly, 8.62 g of 4,4′-ODA and 102 g of DMAc were added into a 250 mL three-neck round bottom flask, and stirred with a mechanical agitator to be dissolved completely. Then, 9.38 g of PMDA was added into the above solution, and stirred at 0 °C for 5 h to obtain the prepolymer of PAA. Subsequently, 4.36 g of TEA was slowly added and stirred for another 5 h to dissolve PAA. Thus, a viscous PAA solution with the solid content of 15 wt% was obtained. It was then slowly poured into deionized water at 0 °C to guarantee adequate solvent exchange of DMAc. Finally, the PAA solid was frozen in liquid nitrogen (−196 °C) and subsequently freeze-dried for further use.

Preparation of BC/PAA, BC/PI aerogels and carbon aerogels

The BC pellicles were firstly immersed into 0.1 M NaOH solution for 6 h, and then washed with deionized water for several times to pH ≈7. Then, the rectangular BC pellicles were frozen in liquid nitrogen (−196 °C) and subsequently freeze-dried. In a typical preparation process of carbon aerogels, 4 g of PAA was dissolved into a mixed solution of 90 g deionized water and 2 g TEA to form a viscous PAA solution. Afterwards, 4 g of the freeze-dried BC membrane was cut into 1×1 cm^2 pieces and dispersed into the above PAA solution by homogenizing the mixture at 18000 rpm for 30 min using an IKA T25 homogenizer, thus yielding a uniform BC/PAA suspension containing 4 wt% BC nanofibers and 4 wt% PAA (with a mass ratio of 1/1 for BC/PI). Then, the suspension was poured into desired molds, frozen in liquid nitrogen (−196 °C), and freeze-dried for 48 h to form BC/PAA aerogel through the fibrous freeze-shaping technique.[7] The obtained BC/PAA aerogel (denoted as BC/PAA-50, where "50" presents the mass percentage of PAA in the BC/PAA aerogel) was further heated up to 300 °C in nitrogen flow with a heating rate of 2 °C min^{-1}, during which process it was respectively kept at 100, 200, and 300 °C for 30, 30, and 60 min for

the complete imidization of PAA into polyimide. At last, the BC/PI-50 aerogel was further heated up to 800 °C at a heating rate of 5 °C min^{-1} and holding at 800 °C for 1 h under N_2 atmosphere to obtain carbon aerogel, which was labeled as BP-50 carbon aerogel. Meanwhile, carbon aerogels derived from BC/PAA aerogels with different BC/PAA mass ratios of 1:0, 7:1, 3:1, 5:3, 0:1 were also obtained using the above procedures, which are denoted as BP-0, BP-12.5, BP-25, BP-37.5, and BP-100 carbon aerogels, respectively.

Characterization

The compression tests of BC/PAA-50, BC/PI-0, 12.5, 25, 37.5, 50 aerogels and BP-50 carbon aerogels were performed using an electronic universal testing machine (CMT 4104) equipped with two flat-surface compression stages at a speed of 2 mm s^{-1}. Cylindrical samples with diameters of ≈18 mm and height of ≈30 mm were used in all compression tests. The morphology of the samples was investigated by field emission scanning electron microscope (FESEM, Ultra 55, Zeiss) at an acceleration voltage of 5 kV. Transmission electron microscopy (TEM) image was observed on a JEOL-2010 transmission electron microscope at an acceleration voltage of 200 kV. The specific surface area was calculated by the conventional Brunauer–Emmet–Teller (BET) method with a belsorp-max surface area detecting instrument (Tristar3000). The pore size distribution was derived from the adsorption branches of isotherms by Barrett–Joyner–Halenda (BJH) method. Phase structure of the sample was conducted by X-ray diffraction (XRD, X'pert PRO, PANalytical) with $Cu_{K\alpha}$ radiation ($\lambda = 0.1542$ nm) at a speed of 5° min^{-1} from $2\theta = 10°$ to 70° under a voltage of 40 kV and a current of 40 mA. X-ray photoelectron spectroscopy (XPS) analyses were carried out on a RBD upgraded PHI-5000C ESCA system (PerkinElmer) with $Mg_{K\alpha}$ radiation ($h\nu = 1253.6$ eV). All XPS spectra were corrected using C 1s line at 284.6 eV while curve fitting and background subtraction were accomplished using a RBD AugerScan 3.21 software. Thermogravimetric analysis (Pyris 1 TGA, PerkinElmer) was performed in air from 100 to 700 °C at a heating rate of 20 °C min^{-1}.

Sorption of oils and organic solvents

In a typical sorption experiment, a carbon aerogel was directly placed in organic liquids or oils until reaching the adsorption equilibrium, and then taken out for weight measurement. Weight gain of the aerogel was calculated according to its weight change before and after adsorption. In order to prevent the evaporation of the adsorbed organic liquid with low boiling points, the weight measurement should be done quickly. All adsorption experiments were conducted three times to get the average sorption capacity. Recycle of carbon aerogels was accomplished by the direct combustion of aerogels in air to remove the adsorbed liquid.

Electrochemical measurements

Prior to all electrochemical measurements, electrodes were prepared according to the previously reported work.[25] Electrochemical measurements were performed in 6 M KOH aqueous solution on an electrochemical working station (CHI660D, Chenhua Instruments Co. Ltd., Shanghai) with a standard three-electrode setup, where the Ag/AgCl and Pt wire were used as the reference and counter electrode, respectively. The working electrode was prepared by mixing the powder of carbon aerogel (milled using a quartz mortar), carbon black and poly(tetrafluoroethylene) in a mass ratio of 80:10:10 to obtain slurry. Then, the slurry was pressed onto the nickel foam current collector and dried at 80 °C for 12 h. Mass loading of the electrode materials was fixed at 3 mg. Cyclic voltammograms (CV) were obtained from −1 to 0 V with different scan rates ranging from 5 to 200 mV s^{-1}. Galvanostatic charge-discharge (GCD) testing was performed between −1 and 0 V under different current densities from 0.5 to 10 A g^{-1}. The electrochemical impedance spectroscopy (EIS) measurements were conducted by applying an AC voltage in the frequency range from 10 mHz to 100 kHz with an amplitude of 5 mV. The specific capacitance (C_s) can be calculated from galvanostatic charge–discharge curves according to Equation (1):

$$C_s = \frac{I \times \Delta t}{m \times v} \quad (1)$$

where I (A) is the current, v (V) is the potential, m (g) is the mass of electroactive materials, and Δt (s) is the discharge time.

Acknowledgements

The authors are grateful for the financial support from the National Natural Science Foundation of China (51125011, 51373037, 51433001).

Keywords: adsorbents · bacterial cellulose · carbon aerogels · polyimide · supercapacitor electrodes

[1] G. Hayase, K. Kanamori, M. Fukuchi, H. Kaji, K. Nakanishi, *Angew. Chem. Int. Ed.* **2013**, *52*, 1986; *Angew. Chem.* **2013**, *125*, 2040.
[2] S. Kabiri, D. N. H. Tran, T. Altalhi, D. Losic, *Carbon* **2014**, *80*, 523.
[3] Y. Lin, T. Wei, H. Chien, S. Y. Lu, *Adv. Energy Mater.* **2011**, *1*, 901.
[4] Z. Wu, S. Yang, Y. Sun, K. Parvez, X. L. Feng, K. Muellen, *J. Am. Chem. Soc.* **2012**, *134*, 9082.
[5] Y. G. Yan, Y. S. Au, D. Rentsch, A. Remhof, P. de Jongh, A. Zuettel, *J. Mater. Chem. A* **2013**, *1*, 11177.
[6] R. J. White, N. Brun, V. L. Budarin, J. H. Clark, M. M. Titirici, *ChemSusChem* **2014**, *7*, 670.
[7] Y. Si, J. Y. Yu, X. M. Tang, J. L. Ge, B. Ding, *Nat. Commun.* **2014**, *5*, 5802.
[8] G. G. Duan, S. H. Jiang, V. Jerome, J. H. Wendorff, A. Fathi, J. Uhm, V. Altstaedt, M. Herling, J. Breu, R. Freitag, S. Agarwal, A. Greiner, *Adv. Funct. Mater.* **2015**, *25*, 2850.
[9] Z. Y. Wu, C. Li, H. W. Liang, Y. N. Zhang, X. Wang, J. F. Chen, S. H. Yu, *Sci. Rep.* **2014**, *4*, 4079.
[10] Y. M. Ren, Q. Xu, J. M. Zhang, H. X. Yang, B. Wang, D. Y. Yang, J. H. Hu, Z. M. Liu, *ACS Appl. Mater. Interfaces* **2014**, *6*, 9689.
[11] Y. Q. Li, Y. A. Samad, K. Polychronopoulou, S. M. Alhassan, K. Liao, *ACS Sustainable Chem. Eng.* **2014**, *2*, 1492.
[12] P. Hao, Z. H. Zhao, J. Tian, H. D. Li, Y. H. Sang, G. W. Yu, H. Q. Cai, H. Liu, C. P. Wong, A. Umar, *Nanoscale* **2014**, *6*, 12120.
[13] X. L. Yao, W. J. Yu, X. Xu, F. Chen, Q. Fu, *Nanoscale* **2015**, *7*, 3959.
[14] N. H. Phan, S. Rio, C. Faur, L. Le Coq, P. Le Cloirec, T. H. Nguyen, *Carbon* **2006**, *44*, 2569.
[15] L. Sun, C. Tian, M. Li, X. Meng, L. Wang, R. Wang, J. Yin, H. Fu, *J. Mater. Chem. A* **2013**, *1*, 6462.
[16] C. Chen, Y. Huang, C. Zhu, Y. Nie, J. Yang, D. Sun, *Chin. J. Polym. Sci.* **2014**, *32*, 439.
[17] S. Ma, Q. Mi, J. Yu, J. He, J. Zhang, *Prog. Chem.* **2014**, *26*, 796.
[18] F. L. Lai, Y. E. Miao, Y. P. Huang, Y. F. Zhang, T. X. Liu, *ACS Appl. Mater. Interfaces* **2015**, DOI: 10.1021/acsami.5b06274.
[19] C. Long, D. Qi, T. Wei, J. Yan, L. Jiang, Z. Fan, *Adv. Funct. Mater.* **2014**, *24*, 3953.
[20] Y. Wang, S. Yadav, T. Heinlein, V. Konjik, H. Breitzke, G. Buntkowsky, J. J. Schneider, K. Zhang, *RSC Adv.* **2014**, *4*, 21553.
[21] Y. F. Zhang, W. Fan, Y. P. Huang, C. Zhang, T. X. Liu, *RSC Adv.* **2015**, *5*, 1301.
[22] C. Ma, J. L. Shi, Y. J. Li, Y. Song, L. Liu, *New Carbon Mater.* **2015**, *30*, 295.

[23] J. H. Zhu, L. W. Mu, L. Chen, Y. J. Shi, H. Y. Wang, X. Feng, X. H. Lu, *Macromol. Chem. Phys.* **2014**, *215*, 1407.
[24] Y. Z. Li, J. Dong, J. X. Zhang, X. Zhao, P. P. Yu, L. Jin, Q. H. Zhang, *Small* **2015**, *11*, 3476.
[25] S. Park, M. Vosguerichian, Z. Bao, *Nanoscale* **2013**, *5*, 1727.
[26] J. H. Fang, H. Kita, K. Okamoto, *Macromolecules* **2000**, *33*, 4639.
[27] X. Ning, W. J. Koyos, *Carbon* **2014**, *66*, 511.
[28] M. D. Gawryla, O. van den Berg, C. Weder, D. A. Schiraldi, *J. Mater. Chem.* **2009**, *19*, 2118.
[29] H. W. Liang, Q. F. Guan, L. F. Chen, Z. Zhu, W. J. Zhang, S. H. Yu, *Angew. Chem. Int. Ed.* **2012**, *51*, 5101; *Angew. Chem.* **2012**, *124*, 5191.
[30] K. H. Kim, Y. Oh, M. F. Islam, *Nat. Nanotechnol.* **2012**, *7*, 562.
[31] H. C. Bi, Z. Y. Yin, X. H. Cao, X. Xie, C. L. Tan, X. Huang, B. Chen, F. T. Chen, Q. L. Yang, X. Y. Bu, X. H. Lu, L. T. Sun, H. Zhang, *Adv. Mater.* **2013**, *25*, 5916.
[32] N. Xiao, Y. Zhou, Z. Ling, J. S. Qiu, *Carbon* **2013**, *59*, 530.
[33] A. Li, H. X. Sun, D. Z. Tan, W. J. Fan, S. H. Wen, X. J. Qing, G. X. Li, S. Y. Li, W. Q. Deng, *Energy Environ. Sci.* **2011**, *4*, 2062.
[34] X. Z. Xu, J. Zhou, D. H. Nagaraju, L. Jiang, V. R. Marinov, G. Lubineau, H. N. Alshareef, M. Oh, *Adv. Funct. Mater.* **2015**, *25*, 3193.
[35] M. Husseien, A. A. Amer, A. El-Maghraby, N. Hamedallah, *J. Anal. Appl. Pyrolysis* **2009**, *86*, 360.
[36] D. Bastani, A. A. Safekordi, A. Alihosseini, V. Taghikhani, *Sep. Purif. Technol.* **2006**, *52*, 295.
[37] X. C. Gui, J. Q. Wei, K. L. Wang, A. Y. Gao, H. W. Zhu, Y. Jia, Q. K. Shu, D. H. Wu, *Adv. Mater.* **2010**, *22*, 617.
[38] Z. Y. Wu, C. Li, H. W. Liang, J. F. Chen, S. H. Yu, *Angew. Chem. Int. Ed.* **2013**, *52*, 2925; *Angew. Chem.* **2013**, *125*, 2997.
[39] S. S. Banerjee, M. V. Joshi, R. V. Jayaram, *Chemosphere* **2006**, *64*, 1026.
[40] R. R. Salunkhe, Y. Kamachi, N. L. Torad, S. M. Hwang, Z. Q. Sun, S. X. Dou, J. H. Kim, Y. Yamauchi, *J. Mater. Chem. A* **2014**, *2*, 19848.
[41] S. Zhong, C. X. Zhan, D. P. Cao, *Carbon* **2015**, *85*, 51.
[42] Q. Wang, J. Yan, Y. B. Wang, G. Q. Ning, Z. J. Fan, T. Wei, J. Cheng, M. L. Zhang, X. Y. Jing, *Carbon* **2013**, *52*, 209.
[43] T. T. Li, N. Li, J. W. Liu, K. Cai, M. F. Foda, X. M. Lei, H. Y. Han, *Nanoscale* **2015**, *7*, 659.

Manuscript received: November 30, 2015
Revised: December 16, 2015
Accepted Article published: December 28, 2015
Final Article published: January 20, 2016